# The STAR Endcap Electromagnetic Calorimeter

C.E. Allgower,[d] B.D. Anderson,[e] A.R. Baldwin,[e] J. Balewski,[d] M. Belt-Tonjes,[f] L.C. Bland,[d] R.L. Brown,[b] R.V. Cadman,[a] W. Christie,[b] I. Cyliax,[d] V. Dunin,[c] L. Efimov,[c] G. Eppley,[h] C.A. Gagliardi,[i] N. Gagunashvili,[c] T. Hallman,[b] W. Hunt,[d] W.W. Jacobs,[d] A. Klyachko,[d] K. Krueger,[a] A. Kulikov,[c] A. Ogawa,[g] Y. Panebratsev,[c] M. Planinic,[d] J. Puskar-Pasewicz,[d] G. Rakness,[d] S. Razin,[c] O. Rogachevski,[c] S. Shimansky,[c] K.A. Solberg,[d] J. Sowinski,[d] H. Spinka,[a] E.J. Stephenson,[d] V. Tikhomirov,[c] M. Tokarev,[c] R.E. Tribble,[i] D. Underwood,[a] A.M. Vander Molen,[f] S.E. Vigdor,[d] J.W. Watson,[e] G. Westfall,[f] S.W. Wissink,[d] A. Yokosawa,[a] V. Yurevich,[c] W.-M. Zhang,[e] A. Zubarev[c]

[a] *High Energy Physics Division, Argonne National Laboratory, Argonne, Illinois 60439, U.S.A.*[2]

[b] *Physics Division, Brookhaven National Laboratory, Upton, New York 11973, U.S.A.*[2]

[c] *Laboratory of High Energy Physics, JINR, 141 980 Dubna, Russia*

[d] *Indiana University Cyclotron Facility, Bloomington, Indiana 47408, U.S.A.*[1]

[e] *Department of Physics, Kent State University, Kent, Ohio 44242, U.S.A.*[1]

[f] *Department of Physics, Michigan State University, East Lansing, Michigan 48824, U.S.A.*[2]

[g] *Department of Physics, Pennsylvania State University, University Park, Pennsylvania 16802, U.S.A.*

[h] *Department of Physics, Rice University, Houston, Texas 77251, U.S.A.*

[i] *Cyclotron Institute, Texas A&M University, College Station, Texas 77843, U.S.A.*[2]

*Preprint submitted to Elsevier Preprint* *20 February 2002*

**Abstract**

The STAR endcap electromagnetic calorimeter will provide full azimuthal coverage for high-$p_T$ photons, electrons and electromagnetically decaying mesons over the pseudorapidity range $1.086 \leq \eta \leq 2.00$. It includes a scintillating-strip shower-maximum detector to provide $\pi^0/\gamma$ discrimination and preshower and postshower layers to aid in distinguishing between electrons and charged hadrons. The triggering capabilities and coverage it offers are crucial for much of the spin physics program to be carried out in polarized proton-proton collisions.

*PACS:* 29.40.Vj; 29.40.Mc; 07.85.+n

*Keywords:* Detectors; Electromagnetic Calorimeter; $\pi^0/\gamma$ Discrimination; Electron/Hadron Discrimination

## 1 Motivation and Requirements

A single endcap electromagnetic calorimeter (EEMC) is presently under construction for installation in 2002-3 on the west poletip of the STAR detector. The EEMC will provide coverage for pseudorapidity values $1 < \eta \leq 2$, over the full azimuthal range, supplementing the barrel EMC (BEMC) described in the preceding article. Within this acceptance, it will add the capabilities to detect photons and electromagnetically decaying mesons ($\pi^0$, $\eta$), to identify electrons and positrons, and to trigger on high-energy particles of these types. The EEMC will include a shower-maximum detector optimized to discriminate between photons and $\pi^0$ or $\eta$ mesons over the 10-40 GeV energy region, as well as preshower and postshower layers intended for electron *vs.* hadron discrimination. Furthermore, it will significantly enhance the acceptance and triggering capabilities of STAR for jets.

The greatest demand for such forward calorimetry arises from the program of experiments to be carried out with colliding polarized proton beams at RHIC [1–3]. One of the most important goals of this program is to determine the helicity preference for gluons [$\Delta G(x_g)$] inside a polarized proton, as a function of the fraction $x_g$ of the proton's momentum carried by the gluon, and to constrain strongly the net gluon contribution to the proton's spin, given by the integral of this quantity over $x_g$. The gluon polarization can be probed in quark-gluon Compton scattering, by measuring longitudinal spin correlations –

[1] Partially supported by the U.S. National Science Foundation under grant numbers PHY-9602872, PHY-9977216, PHY-9971947 and others.

[2] Supported by the U.S. Department of Energy under grant numbers W-31-109-ENG-38, DE-FG03-93ER40765, and others.

the difference divided by the sum of cross sections for equal *vs.* opposite beam helicities – for direct photon production at transverse momentum transfers $p_T \gtrsim 10$ GeV/c. The endcap calorimeter adds crucial coverage for asymmetric partonic collisions, where both the photon and the away-side jet resulting from the final-state quark are boosted forward in the collider frame. These collisions are of particular importance because they permit exploitation of the highly polarized quarks at momentum fractions $x_q \gtrsim 0.2$ in one proton, to probe the gluon polarization in the other proton at $x_g < 0.1$, where the vast majority of gluons reside [2,3]. In such asymmetric collisions, both the photon and many jet fragments are typically detected in the endcap region. The EEMC will also significantly enhance STAR's sensitivity to the flavor-dependence of sea antiquark polarizations via $W^{\pm}$ production in polarized p-p collisions [3,4]. When the high-$p_T$ daughter $e^{\pm}$ from W-boson decay is detected in the EEMC, the kinematics of the production and decay processes permit the cleanest extraction of both the $x$-values and separate polarizations of the colliding quark and antiquark. The $q$ *vs.* $\overline{q}$ polarizations can be determined by measuring the independent (parity-violating) sensitivities of the $W^{\pm}$ yield to helicity-flip of one *vs.* the other polarized beam.

The above physics opportunities set the requirements for the EEMC. Some of the most important of these are summarized in Table 1, together with the physics goals that drive them. In particular, we note the need to cover a very wide dynamic range (nearly 1000:1 in energy), with excellent $\pi^0/\gamma$ and hadron/electron suppression, and accurate absolute calibration of the calorimeter energy scale. The focus on p-p rather than A-A collisions relaxes somewhat the demand on tower segmentation, in comparison with the STAR BEMC. These requirements then dictate a tradeoff, in which the granularity of readout channels for the calorimeter towers is reduced, but a more expensive scintillator solution is used for the shower-maximum detector (SMD). For the higher-energy showers that characterize the $p_T$ range of interest in the endcap $\eta$ region, the scintillator SMD promises significantly better performance, in both transverse shower profile delineation and energy deposition resolution, than the gaseous BEMC SMD counters.

## 2 Tower Structure and Optical Chain

We have chosen a traditional Pb/plastic scintillator sampling calorimeter for the EEMC design, primarily due to advantages in cost, simplicity and sharing of technology with STAR's BEMC. The actual pseudorapidity range covered is $1.086 \leq \eta \leq 2.00$, leaving a small gap between the endcap and barrel calorimeters, needed for services to exit the solenoid. The full annulus will be divided into two halves, with one shown in Fig. 1. The geometry of the alternating Pb radiator and scintillator layers is illustrated in the lower portion of the fig-

Table 1
Some requirements on EEMC coverage and performance

| **Feature** | **Requirement** | **Driving Physics Goals** |
|---|---|---|
| Geom. Acceptance | $1 \lesssim \eta \leq 2$; full $\phi$ | $\gamma$+jet sensitivity to $0.01 \lesssim x_g \lesssim 0.3$ |
| $E_{min}$ in One Tower | $\approx$0.2 GeV | MIP's for calibration; $\gamma$'s from asymmetric $\pi^0$ decay; $\approx$2% shower leakage from $p_T = 10$ GeV/c $\gamma$'s |
| $E_{max}$ in One Tower | 150 GeV | $e^{\pm}$ from $W^{\pm}$ decay at $\eta = 2$ |
| Linearity | $< 10\%$ integral non-linearity, $\sim$1–150 GeV | correct to give $W^{\pm}$ daughter $p_T$ to $\pm 1$ GeV/c from lower-E calibrations |
| Depth | $\geq 20X_0$, $\leq 1$ hadron interaction length | $< 10\%$ shower leakage for 150 GeV $e^{\pm}$; minimize hadron sensitivity to fit within existing space |
| Energy Resolution | $(\frac{\sigma_E}{E}) \leq (\frac{16\%}{\sqrt{E}}) + (2\%)$ | $x_{\overline{q}}$ uncertainty $\lesssim \pm 0.01$ for $W^{\pm}$ reconstruction at $p_{T,e} \leq 30$ GeV/c |
| $\gamma/\pi^0$ Discrimination | $\pi^0/\gamma$ suppress factor $> 3$ for $p_T \approx 10 - 20$ GeV/c $\Rightarrow$ SMD | keep background subtraction from enlarging $\Delta G(x)$ errors by more than a factor of 2 |
| $e^{\pm}/h^{\pm}$ Discrimination | suppress $h^{\pm}/e^{\pm}$ by $> 10$ for $p_T \gtrsim 5$ GeV/c $\Rightarrow$ pre/post-shower | reach $> 3:1$ W signal/hadronic bkgrd. ratio for $p_T > 20$ GeV/c; enhance Drell-Yan signal/bkgrd. |
| Jet Reconstruction | $\sigma \approx 0.1$ for $\eta_{jet}$, $\phi_{jet}$ | reconstruct $x_{1,2}$ values for colliding partons in $\gamma$+jet coinc. to $\approx \pm 0.01$ |
| Segmentation/ Rate Capability | tower occupancy $< 10\%$ @ $L_{pp} = 2 \times 10^{32}$; tower size $\gtrsim 2 \times$ shower diam. | trigger on isolated $\gamma$ or $e^{\pm}$ *vs.* jet; minimize tower hadron occupancy; obey WLS fiber min. bend radius |
| Tower Calibration | absolute E calibration to $\pm 2\%$ ($\pm 10\%$ online) | minimize: systematic errors in $x_g$, $\int \Delta G(x)dx$ ($p_T$, hence $x$, threshold at acceptable trigger rates) |
| Coverage Gaps | $< 2\%$ systematic shower E loss in cracks | minimize systematic errors in extracted $x_g$, $\int \Delta G(x)dx$ |
| SMD Calibration | relative gains of adjacent strips known to $\lesssim \pm 10\%$ | maintain sufficient $\gamma$ *vs.* $\pi^0$ shower shape discrimination |
| Timing Response | $< 1$ RHIC beam period (110 ns) | aid TPC pileup reject; no occupancy from neighboring beam crossings |

ure. A scintillator strip shower maximum detector (SMD) with high position resolution is located after the 5th radiator plate. Light from the towers and SMD is carried on optical fibers outside the STAR magnet, to photomultiplier tubes mounted on the rear of the poletip. The EEMC is supported from a strong stainless steel backplate, which attaches to the poletip, and a terraced, conical stainless steel hub at the inner radius, to which the radiator sheets are attached.

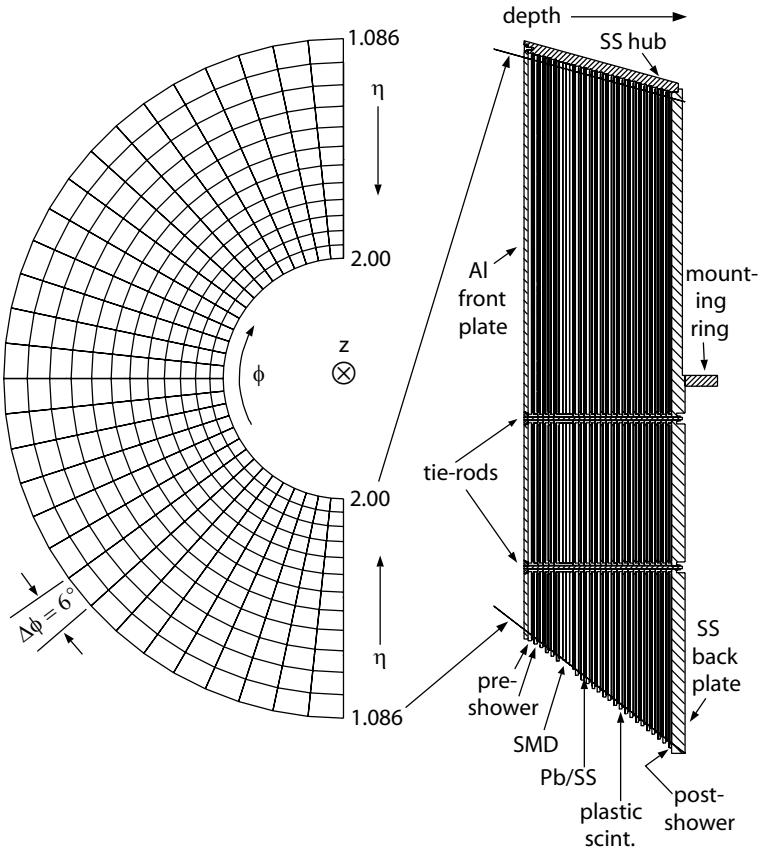


Fig. 1. *Schematic EEMC tower structure. The left-hand view shows the subdivision into half of the total 720 towers. The towers are projective, with edges aligned with the center of the beam intersection region, 2.7 m distant along the z-axis from the EEMC front face. Towers span* $\Delta\phi = 0.1$ *in azimuthal angle, and varying size in pseudorapidity (*$\Delta\eta = 0.057$ *to 0.099). The two halves of the EEMC will actually be mounted in STAR with their dividing line* $15^\circ$ *away from horizontal. The right view, drawn with a different scale, represents a cross section at constant* $\phi$*, showing the depth (z-) profile of the calorimeter and the structural tie-rods used at* $30^\circ$ *intervals in* $\phi$*. Each tower has 23 layers of lead/stainless steel absorber interleaved with 24 layers of plastic scintillator. Also indicated are the preshower, post-shower and shower-maximum detector layers, and the stainless steel mounting ring that will be inserted into a poletip recess to partially support the weight of the lower half EEMC.*

A standard layer of the calorimeter consists of Pb/stainless steel laminate followed by a 4-mm thick (Kuraray SCSN-81) plastic scintillator. Each radiator sheet comprises 4.57-mm thick calcium-loaded Pb sheets laminated on each

face with 0.5 mm stainless steel, for a total of $\approx 0.85$ radiation lengths. The four specially configured layers providing preshower, postshower and SMD functions are described in later sections. The total mass of the radiator sheets and active elements, for the two EEMC halves combined, is $\approx 25000$ kg. Following designs of endcap subsystems in both the D0 [7] and CDF [8] detectors, the large loads are carried by stainless steel – ultimately by the back plate and hub – with the Pb serving as filler in the laminated radiator plates. Additional structural integrity is provided by tie-rods that bolt the aluminum front plate to the back plate at two radii along radial lines every 30° in azimuth (see Figs. 1 and 3). These tie-rods pass through stainless steel inserts in every radiator sheet, and naturally divide the detector into 30° modules. The whole assembly represents 21.4 radiation lengths at normal incidence and provides a shower energy sampling fraction of 6.6%, resulting [3] in sufficient energy resolution and depth to measure electromagnetic shower energy at the levels needed for the physics program sketched above. In addition, there is an average of $\sim$1 radiation length of material in the STAR detector preceding the EEMC along the particle trajectories. On the other hand, the entire assembly corresponds to slightly less than one hadronic interaction length.

The tower segmentation is produced using megatile construction, as developed for CDF [5] and adopted for the BEMC [6]. In the EEMC, megatiles span either 6° or 12° in azimuthal angle ($\phi$), with machined isolation grooves separating each into 12 or 24 trapezoidal tiles, respectively. One 30° sector of a calorimeter layer contains two 12° megatiles, aligned flush against the tie-rods on each side, and a 6° "keystone" megatile. Loss of shower energy in the cracks between megatiles and near the tie-rods is minimized by a slight azimuthal staggering of the megatiles in successive layers, accomplished by means of small tailored notches cut in the 12° megatile edges that engage the tie-rods (similar to, but smaller than, the SMD tie-rod notches shown in Fig. 3). Dead regions are further limited by mounting the two halves of the EEMC with the dividing line 15° from horizontal, so that the tie-rods are aligned with the thick spokes that define the 30° azimuthal sector structure in the endcap of the STAR TPC.

Wavelength-shifting (WLS) optical fibers (Kuraray Y11-doped 200 ppm fiber of 0.83 mm diameter), inserted into $\sigma$-shaped grooves machined in the face of each tile, run through channels in a white plastic fiber-routing layer (FRL) out to the $\eta \approx 1$ edge of each megatile. A photograph of one megatile and its accompanying FRL is shown in Fig. 2. Wiggles machined in the FRL channels take up slack in fiber length, permitting use of equal length WLS fibers for every layer within a given tower, despite the projective geometry. This choice meets the uniformity requirement on light output from the different tiles in a tower, while maintaining convenience in the preparation of WLS fiber bundles.

At the edge of each megatile, optical connectors couple the WLS fibers from

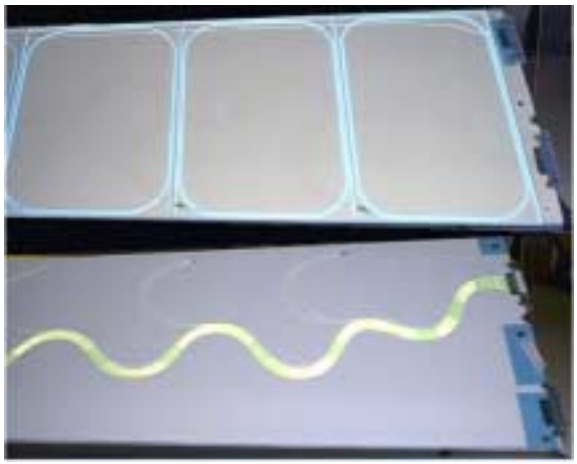

Fig. 2. *Closeup photographs near the $\eta = 1$ edge of an assembled 6° megatile. The upper photo shows the machined isolation and $\sigma$-shaped grooves in the scintillator and, running near the upper edge, the "leaky" UV-transparent fiber used to illuminate each tile with diagnostic laser pulses. The lower photo shows the opposite side of the fiber-routing layer, with wavelength-shifting fibers routed through undulating channels, from which they enter the $\sigma$ grooves in each tile.*

the 12 tiles within a given 6° sector to 0.9-mm diameter clear fibers, which then run to the rear of the STAR poletip. There the clear fiber bundles from each of the 24 scintillator layers within a given 6° sector are connected to a common steel box housing the 12 (Electron Tubes Limited model 9107B) photomultiplier tubes (PMT) for the towers in that sector. Within each PMT box, a fiber harness, composed of 1-mm diameter clear fibers of 20–45 cm length reroutes the light from megatile groupings to tower groupings. Light from the 24 layers within each tower is combined via an optical mixer in a single PMT, to produce a signal proportional to the total energy deposited in that tower. The PMT's are powered by Cockroft-Walton bases which, when supplied externally with 130 V DC, generate a specially tapered high voltage distribution for the dynodes. At a gain of $2 \times 10^5$, these PMT's provide a response linear to within $\pm 2\%$ for peak pulse currents from zero to at least 50 mA (corresponding to shower energies $\sim$100 GeV). With the full optical chains and PMT's to be used in the installed detector, cosmic ray muons passing through one of the 4-mm scintillator tiles at normal incidence typically produce an average of 2.3–3.2 (depending on WLS fiber length) photoelectrons at the PMT photocathode. This performance is sufficient to meet the tower resolution requirements.

## 3 Shower-Maximum Detector Design and Performance

Placed about five radiation lengths deep within the EEMC is a specially configured layer designed to provide the fine granularity crucial to distinguishing the transverse shower profiles characteristic of single photons *vs.* the close-lying photon pairs from $\pi^0$ and $\eta^0$ decay. The depth of this layer is chosen to optimize the discrimination, by compromising between statistical definition of the profile measurement (maximized at somewhat greater depth) and degree of overlap of the two daughter photon showers (worsening with increasing

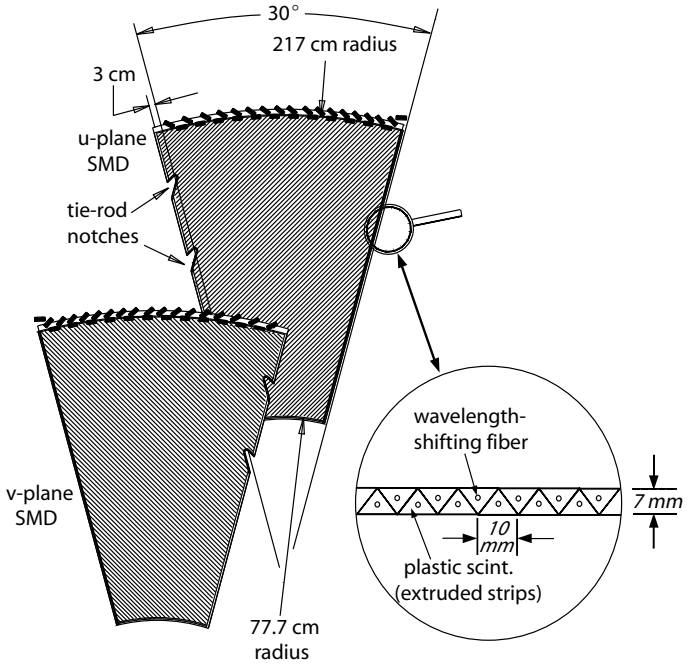


Fig. 3. *Layout of one 30° sector of the SMD. Each of the two orthogonal planes will be constructed from triangular scintillating strips extruded with an axial hole for the wavelength-shifting fiber.*

depth). This shower-maximum detector (SMD) will also be useful in $e$/hadron discrimination and the matching of $e^{\pm}$ hits to TPC tracks. The SMD is made of extruded polystyrene-based scintillator strips of triangular cross section, organized into orthogonal $u$ and $v$ planes as shown schematically in Fig. 3. The triangular cross section results in a sharing of the energy deposition among adjacent strips that enhances the position resolution and the stability of the measured shower profile shape. Such a design and similar techniques have been developed by D0 for use as a tracking preshower detector [9]. The SMD scintillators are segmented into (nominally) 30° modules, each of which has notches cut on one radial edge, which permit most of the strips to extend a few cm in length beyond the structural tie-rods. Adjacent $u$- or $v$-sectors are then offset longitudinally to permit overlap in their azimuthal coverage, permitting an essentially gapless (except very near the tie-rods) detector to be assembled from three layers of 36 mm total depth. Each 90° azimuthal segment of each of the three SMD layers contains one active $u$-plane and one active $v$-plane module, plus one plastic spacer module spanning slightly less than 30°.

Light from the SMD is carried by WLS fibers that run along the length of each strip, through axial holes of 1.0-mm diameter created during the extrusion. These fibers exit either directly at the outer circumference of the SMD, where they are bunched into 8-fiber optical connectors, or along the radial sector edge opposite the tie-rod notches, whence they bend around to run to the outer circumference through a grooved FRL mounted on the surface of the scintillator strip plane. The latter WLS fibers are coupled at the outer circumference to clear fibers via 12-fiber optical connectors. The clear fibers transport the light to 16-anode PMT's (Hamamatsu R5900-M16) housed in steel boxes on

the rear of the STAR poletip. Three such boxes, containing 12 multi-anode tubes (MAPMT) apiece, along with their Cockroft-Walton bases and front-end electronics, service the 572 total strips (286/plane) in each 30° SMD sector. The mapping of SMD fibers to MAPMT pixels is chosen to minimize the probability that the small ($\sim 1\%$ in amplitude) crosstalk among neighboring pixels can modify the apparent transverse shower profile in a physically significant way. Cosmic ray tests of prototype SMD planes have revealed that a minimum-ionizing particle (MIP) typically yields 0.6 photoelectrons at the MAPMT photocathode per mm of strip thickness traversed.

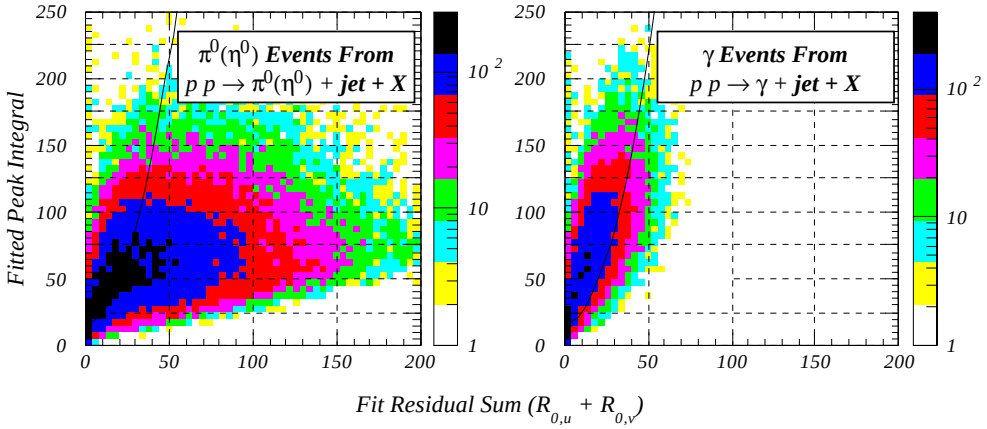


Fig. 4. *Two-dimensional SMD response distributions used to distinguish $\gamma$ from $\pi^0$ ($\eta^0$) events detected in the EEMC. Events simulated with PYTHIA [10] for the two reactions shown at $\sqrt{s_{pp}} = 200$ GeV, both for the same integrated luminosity, have been subjected to kinematic and isolation cuts designed to emphasize $\gamma$-jet coincidences in STAR. The shower profiles simulated with GEANT were fitted with a lineshape consistent with the average simulated SMD response for* single *photons. The y-axis in the plots represents the integral under this fitted lineshape, summed for each event over the u and v SMD planes. The x-axis is a similar sum of "sided" fit residuals, evaluated in each plane for that side of the peak where the fit deviates most from the data, as it would in the presence of a second peak. Roughly 80% (20%) of the photon (meson) events fall above the curve drawn in both frames.*

With the latter light output, simulations have demonstrated [3] that 80% of $\pi^0$'s in the energy range 10-40 GeV can be rejected, while 80% of similar energy photons are retained, by the discrimination algorithm represented in Fig. 4. This performance, when combined with isolation cuts to reject events in which a $\pi^0$ is part of a surrounding jet, is sufficient to achieve the background suppression needed to probe the gluon contribution to the proton's spin via direct photon production in polarized p-p collisions. Improved $\gamma$ retention may be attainable by subjecting apparent two-photon events to an invariant mass cut, using the energy and position of the two SMD clusters.

The shower development predicted for our geometry by GEANT has further-

more been compared to measurements made in two test beam illuminations of a 12-tower prototype of the EEMC, including an SMD layer with $x$ and $y$ strips read out by MAPMT's. These tests were carried out at the Final Focus Test Beam at SLAC, with beams of 5, 10 and 20 GeV electrons delivered in pulses containing typically 1–2 electrons apiece. The prototype detector was scanned across the beam, both horizontally and vertically, to map out the position-dependence of its response.

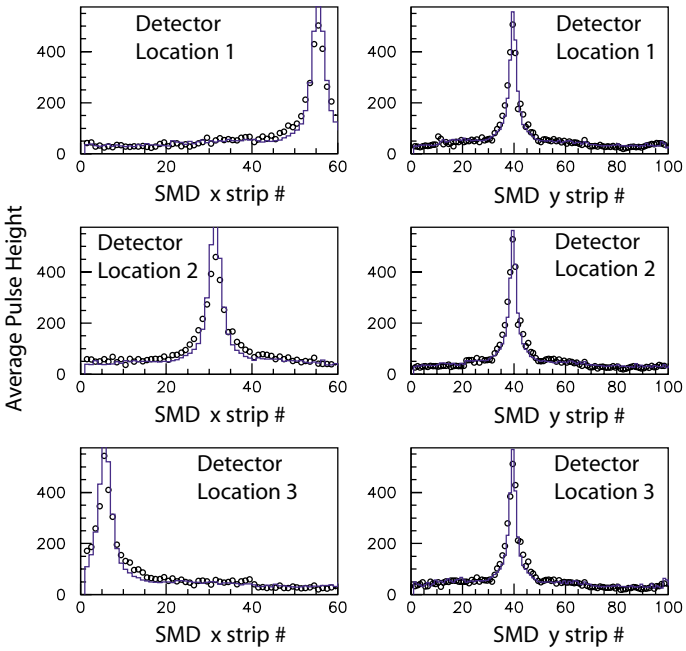


Fig. 5. *Average electromagnetic shower profile, as measured by the $x$- (left) and $y$-(right) planes of the prototype SMD at SLAC. The points are the measured average pulse heights for 5 GeV single-electron events, while the solid-line histograms result from simulations. The upper, middle and lower frames correspond to three different horizontal detector locations.*

For the first test beam run, in October 1999, the prototype SMD layer was constructed from triangular scintillating strips of only 5 mm apex-to-base height, obtained from the D0 collaboration. The applicability of the shower simulations, as well as some problems, are revealed in Fig. 5, which shows the pulse height response of every strip, averaged over many single-electron events at 5 GeV, for three different detector locations with respect to the beam. Most importantly, the transverse shower profile measured by the (downstream) $y$-plane is *quantitatively* reproduced by our simulations, which are based on GEANT-generated shower development and include the influence of photostatistics and intrinsic MAPMT resolution and crosstalk. In contrast, the observed shower profiles in the (upstream) $x$-plane are slightly broader than the simulations. Consistent results were obtained with strips of the final design geometry in the second SLAC run (January 2001). The origin of the differences between the

two planes is currently being investigated. Measurement of the SMD response to $\pi^0$'s will be provided during the 2001 RHIC run, for which the prototype EEMC is installed in a far forward location in STAR.

## 4 Preshower/Postshower Layers

The first two layers of scintillator tiles behind the EEMC front plate, and the last layer as well, are each to be read out by two independent WLS fibers inserted in the (deeper than normal) $\sigma$-grooves. For each tile, the light transported by one of these fibers is added to that from the other depth layers at the tower PMT. Light carried by the second fiber is read out separately, in one (Hamamatsu R5900-M16) MAPMT channel per tile, to form a preshower or postshower detector. Comparison of the light from these tiles to that from the tower as a whole aids in distinguishing electrons from hadrons by exploiting their strong differences in shower probability and longitudinal shower development. The preshower layers also improve the $\pi^0/\gamma$ discrimination for the highest energy photons of interest, since it is roughly twice as likely for a $\gamma$ as for a similar energy $\pi^0$ to deposit no energy in these layers. To achieve adequate photostatistics for both these applications, the pre/postshower layers will be made from thicker (5 mm), brighter (Bicron BC400) scintillator than the normal megatiles. The dopant concentration in the WLS fibers used for summing with the tower light is then to be adjusted to match the light output (for a given energy deposition) to normal layers within the tower.

Simulations indicate that a cut on EEMC preshower energy loss should be capable of suppressing the hadron/electron ratio by a factor $\approx 4.5$ within the 5–30 GeV/c momentum range. A condition on postshower energy should provide an additional factor of 2 suppression, as is also obtainable independently from a cut on the ratio of SMD-to-tower energy. This discrimination provided by the EEMC alone is very important in the endcap region, where deterioration in TPC tracking resolution compromises the otherwise powerful suppression provided by comparing $p_T$ determined in the TPC with transverse energy ($E_T$) detected in the calorimeter. For $W^{\pm}$ and Drell-Yan dilepton production, another powerful condition can be imposed by an isolation cut around the electron candidate. Simulations indicate [3] that an isolation cut suppresses the abundant hadron background for $W^{\pm}$ production by an additional order of magnitude, as does an independent cut rejecting (dijet) events with a sizable energy deposition in the azimuthal region opposite the electron candidate. For $\pi^0/\gamma$ discrimination, the preshower detector can provide extra suppression of the ratio by a factor $\approx 2$, but at the expense of substantially reduced statistics in the surviving $\gamma$ sample.

## 5 Front-End Electronics and Triggering

The tower readout and trigger electronics developed for the BEMC (see preceding article) are being adapted without significant modification for the EEMC tower readout. Allowance for triggers of interest for the spin program is already included in these electronics. Pulse height information from the EEMC towers will be digitized in 12-bit flash ADC's for every RHIC beam crossing and stored in digital pipelines for subsequent processing. The STAR level 0 trigger can compare individual tower ADC values and multi-tower sums to various thresholds and search for simply correlated information from other detector subsystems. The primary trigger for high-$p_T$ direct photon and $W^{\pm}$ production events will be the recording of a very high $E_T$ in a single tower. Jets of interest will be signaled by large $E_T$ and large charged-particle multiplicity (as measured in the Central Trigger Barrel and the Multi-Wire Chamber at the end of the TPC) observed in extended, correlated detector regions. For events that pass the trigger, recording of the full ADC information for individual towers will provide adequate energy resolution and dynamic range to include both single MIP's (*e.g.*, charged hadrons that do not shower) and electrons up to 150 GeV.

A special front-end electronics system for reading out the SMD, preshower and postshower MAPMT's is currently under development for the EEMC. Each MAPMT anode will feed an independent preamplifier, gated integrator and 10-bit ADC (of remotely adjustable conversion gain) to digitize the signals for every beam crossing. 192 channels of such electronics, together with a multiplexer board to provide buffering and simple manipulations on the digitized data, reside in the same steel box as the 12 MAPMT's they service. The MAPMT information is not presently envisioned for use in the level 0 trigger, but will be available for use at level 2, *e.g.*, to allow the possibility of hadron suppression, as needed to achieve manageable trigger rates for $J/\psi$ or low-mass dilepton pair production studies in p-p collisions.

The slow STAR TPC drift velocity poses a special problem for p-p collisions at the expected luminosities ($\sim 10^{32}$ cm$^{-2}$s$^{-1}$). Any desired trigger event will be accompanied by (as many as a few thousand) pileup track segments recorded in the TPC from several hundred beam crossings before and after the one that produced the trigger. Level 3 trigger processors [11] will then be used to prune the pileup tracks and otherwise reduce the data volume transferred to permanent storage. Matching of TPC tracks to the prompt EMC hits, permitting rapid estimation of the event vertex, will provide a critical part of the algorithm that removes TPC clusters along tracks which mate neither to fired EMC towers nor to the event vertex.

## 6 Calibration Systems

Achievement of the stated spin physics goals requires that absolute shower energies be determined from calorimeter tower pulse heights eventually to the $\pm 2\%$ level. The ultimate calibrations will be performed *in situ* within STAR, *e.g.*, by reproducing the known invariant masses of $\pi^0$ and $Z^0$ from detected decay daughters, with crosschecks provided by reconstruction of broader resonances, such as the $\rho^{\pm}$. However, matching of tower gains to $\pm 10\%$ is essential *before* first taking beam, in order to fit the desired spectral landmarks within the tight dynamic range of each readout channel, and to avoid domination of trigger rates by high-gain channels. The relative gains of different SMD strips and pre/postshower tiles must be known eventually to $\pm 10\%$ to achieve the desired performance in $\gamma/\pi^0$ and $e/h$ discrimination. Since these counters are not to be used in the level 0 trigger definition, their hardware matching requirement is dictated by fitting the interesting dynamic range within the allotted 10 bits, despite large channel-to-channel gain fluctuations introduced by the MAPMT's and wide variations in WLS fiber length. Compensation for these fluctuations must be provided at the $\pm 20\%$ level via ADC conversion gain adjustments. In addition, the gain stability of each tower, SMD, pre- and postshower channel must be carefully monitored throughout the useful lifetime of the calorimeter, to allow sudden failures to be revealed promptly and slow deterioration to be tracked.

The present plan calls for three complementary diagnostic and monitoring systems to inject calibrated energies at various stages in the readout chains:

- An externally triggerable pulsed UV laser will be used to inject 355 nm light directly into every scintillating tile of all calorimeter towers. The UV pulses will be delivered via "leaky" (abraded) UV-transparent optical fibers running radially inward through the fiber-routing layer for each megatile. This system will allow nearly complete monitoring of the optical chain for the towers and the pre/postshower layers. An adjustable attenuator at the laser output permits linearity checks of the tower readout over the entire dynamic range. The light intensity from the laser to the towers will be simultaneously monitored in PMT's also viewing calibration $\alpha$-sources embedded in pieces of scintillator. Variable beamsplitters can be used to inject laser pulses into selected tower layers for diagnostic checks, or to otherwise vary the longitudinal profile of injected energy in a tower.
- Pulsed LED's will flash light directly into each tower PMT and one pixel of each pre/postshower MAPMT, to monitor their stability over time. Similar LED's take the place of the laser for the SMD, injecting light pulses into the WLS readout fibers to monitor most of the optical chain for each channel.
- A 300 $\mu$Ci $^{60}$Co source mounted on the end of a long thin rod will be manually insertable through the calorimeter's light-tight skin to inject $\gamma$-

rays into all SMD strips and the tower layers near the SMD in depth. The source can be routed through radial holes in the plastic spacer layers within the SMD, when the poletip is decoupled from the rest of STAR. The peak currents measured for each channel during source scans will allow absolute calibrations performed in one geographical location to be transferred to another.

The absolute energy scale for the full EEMC will be set by cosmic rays studied with a horizontal detector orientation, will be extended over the entire dynamic range using the laser system, and will be transferred between different geographical locations with the aid of the $^{60}$Co source (primary method) and cosmic rays measured in vertical orientation (secondary method). The entire calibration scheme will be checked against test beams for a small prototype detector, but not for an entire EEMC half.

## 7 Summary

The plan is to install the lower half of the EEMC in STAR during the summer 2002 RHIC shutdown, and the upper half a year later. In combination with parallel progress on the BEMC, this will give STAR extensive electromagnetic calorimetry coverage to complement charged particle tracking in the TPC. These new subsystems will greatly enhance STAR's measurement and triggering capabilities in the characterization of particle spectra at high $p_T$, in nucleus-nucleus, proton-nucleus and polarized proton-proton collisions.

## Acknowledgement

We gratefully acknowledge the groundwork laid in earlier designs of the STAR EEMC by Tom Fornek, Ed Bielick and Steve Heppelmann. Valuable advice for the present design was provided by Jim Kerby, Alan Bross, Giorgio Appollinari, Sebastian White, John Martin, David Hertzog, Bernhard Mecking, Mike Lindgren, Don Lincoln, Jim Crittenden and Bill Edwards. We have benefitted considerably from developments for the STAR barrel EMC led by Tom Cormier, Dick Jared, Bob Minor, Jose Riso, Oleg Grachov and Vahe Ghazikhanian. Ted Fieguth and Rick Iverson provided invaluable help for the SLAC beam tests of the prototype EEMC. Anna Pla and Kerry Mellott gave us expert assistance with scintillating material preparation for the SMD strip extrusion. Important contributions to the design and construction of EEMC components have been made by Allan Eads, Barry Phillips, Felipe Franchini,

Tom Kasprzyk and Al Wantroba. We are also grateful to the entire STAR collaboration for their support of this project.

## References

[1] G. Bunce, N. Saito, J. Soffer and W. Vogelsang, Annu. Rev. Nucl. Part. Sci. **50**, 525 (2000).

[2] L.C. Bland, preprint *hep-ex/0002061*.

[3] L.C. Bland *et al.*, STAR Note 401 (1999).

[4] S.E. Vigdor in *Proc. SPIN2000 Conference*, Osaka, October 2000.

[5] S. Kim, Nucl. Instr. Meth. A**360**, 206 (1995).

[6] *Technical Design Report for the Barrel EMC in STAR* (1998), available at web site http://www.star.bnl.gov/STAR/html/emc_l/emc.html.

[7] W. Edwards, private communication.

[8] G. Apollinari, P. de Barbaro and M. Mishina, in Proc. 4th Intl. Conf. on Calorimetry in High Energy Physics, Elba, 1993; CDF II Technical Design Report, FNAL Pub-96/390-E, see http://www-cdf.fnal.gov/upgrades/tdr/tdr_8_plug_cal.html.

[9] M. Adams *et al.*, Nucl. Instrum. Meth. A**378**, 131 (1996).

[10] T. Sjöstrand, Comp. Phys. Commun. **82**, 74 (1994).

[11] J.S. Lange *et al.*, Nucl. Instrum. Meth. A**453**, 397 (2000).